PCCP

Non-Aufbau orbital ordering and spin density modulation in high-spin donor$-$acceptor conjugated polymers

Journal:	*Physical Chemistry Chemical Physics*
Manuscript ID	CP-ART-05-2022-002355.R1
Article Type:	Paper
Date Submitted by the Author:	07-Sep-2022
Complete List of Authors:	Sabuj, Md Abdus; Mississippi State University, Dave C. Swalm School of Chemical Engineering and Center for Advanced Vehicular Systems; Muoh, Obinna; Mississippi State University, Dave C. Swalm School of Chemical Engineering Huda, Masrul; Mississippi State University, Chemical Engineering Rai, Neeraj; Mississippi State University, Dave C. Swalm School of Chemical Engineering

Journal Name

ARTICLE TYPE

Cite this: DOI: 00.0000/xxxxxxxxxx

Non-Aufbau orbital ordering and spin density modulation in high-spin donor−acceptor conjugated polymers†

Md Abdus Sabuj, Obinna Muoh, Md Masrul Huda, and Neeraj Rai*

Received Date
Accepted Date

DOI: 00.0000/xxxxxxxxxx

High-spin ground-state organic materials with unique spin topology can significantly impact molecular magnetism, spintronics, and quantum computing devices. However, strategies to control the spin topology and alignment of the unpaired spins in different molecular orbitals are not well understood. Here, we report modulating spin distribution along the molecular backbones in high-spin ground-state donor−acceptor (D−A) conjugated polymers. Density functional theory calculation indicates substitution of different heteroatoms (such as C, Si, N, and Se) alters the aromatic character in the thiadiazole unit of the benzobisthiadiazole (BBT) acceptor and modulates the oligomer length to obtain a high-spin triplet ground-state, orbital and spin topology. The C, Si, and Se atoms substituted polymers show a localized spin density at the two opposite ends of the polymers. However, a delocalized spin distribution is observed in the N substituted polymer. We find that the hybridization (sp^3 *vs.* sp^2) of the substituent atom plays an important role in controlling the electronic structure of these materials. This study shows that atomistic engineering is an efficient technique to tune the spin topologies and electronic configurations in the high-spin ground-state donor−acceptor conjugated polymers, compelling synthetic targets for room-temperature magnetic materials.

1 Introduction

Open-shell organic semiconductors (OSCs) with a high-spin ($S \geq 1$) ground-state and localized spin topology defy the perpetual notion of spin-pairing as in chemical bonds and are widely utilized in numerous emerging optoelectronic and magnetic applications. OSCs with two (diradicals) or more number of unpaired electrons (polyradicals) have unique optical, electronic, spin-transport, and magnetic properties, making them suitable for potential applications in organic photovoltaic, solar cells, charge-storage devices, organic spintronics, and magnetic materials.[1–9] Research endeavors mostly directed towards finding novel organic high-spin state molecules[10–17] to understand the core mechanism of magnetism which may facilitate the development of new technologies with improved optoelectronic and magnetic properties.[5,18]. However, the mechanism to control their spin distribution and alignment of the unpaired electrons in the MOs are not well studied.[9,19–23]

The unpaired electrons in an open-shell OSCs can be in a spin-paired low-spin singlet ($S = 0$) ground-state or both spins can be aligned in spin-parallel high-spin triplet ($S = 1$) state, overcoming the effect of double-spin polarization.[19,20,24] The relative preferences of a low- and high-spin as ground-state can be controlled by the electron distribution along the molecular backbone.[5,9,20,25,26] The closed-shell materials with a low-spin ground-state tends to accumulate the spin density at the core of the molecular backbone,[20] whereas, the open-shell materials with high-spin ground-state show either a delocalized[19,21] or end localized orbital topology.[20] However, spin-ordering at room temperature is controlled by the magnitude of spin localization, as observed in the edge-modified graphene nanoribbons (GNRs) or zigzag edge graphene nanoribbons (ZGNRs).[27–29] Our recent study on conjugated donor−acceptor (D−A) polymers indicate an end localized spin topology facilitates a high-spin ground-state with a significant population of triplet state at room temperature,[20] which can be synthetic targets for room temperature magnetic materials in the pristine form. This indicates not only the ground-state of OSCs but also their spin-ordering can be manipulated by the spin distribution along the material's backbones. Therefore, controlling the spin topology and spin alignment in the alternating D−A polymers is in the best interest of spintronics and magnetic devices.

The ordering of electrons in the molecular orbitals (MOs) follows the widely accepted Aufbau principle, which states the lowest energy orbitals are filled first, and the singly occupied MOs (SOMOs) should be higher in energy than the highest occupied MOs (HOMOs). However, there are exceptions (Fig. 1a–c) of this widely accepted principle, where implications of the non-Aufbau principle are realized due to the unusual SOMO–HOMO

* *Dave C Swalm School of Chemical Engineering, and Center for Advanced Vehicular Systems, Mississippi State University, Mississippi State, Mississippi, USA 39762. Fax: +1 662 325 2482; Tel: +1 662 325 0790; E-mail: neerajrai@che.msstate.edu*

† Electronic Supplementary Information (ESI) available: [Optimized ground-state geometric parameters, $NICS_{iso}(1)$ values, MO diagrams, spin density diagrams are provided in the supporting information.]. See DOI: 00.0000/00000000.

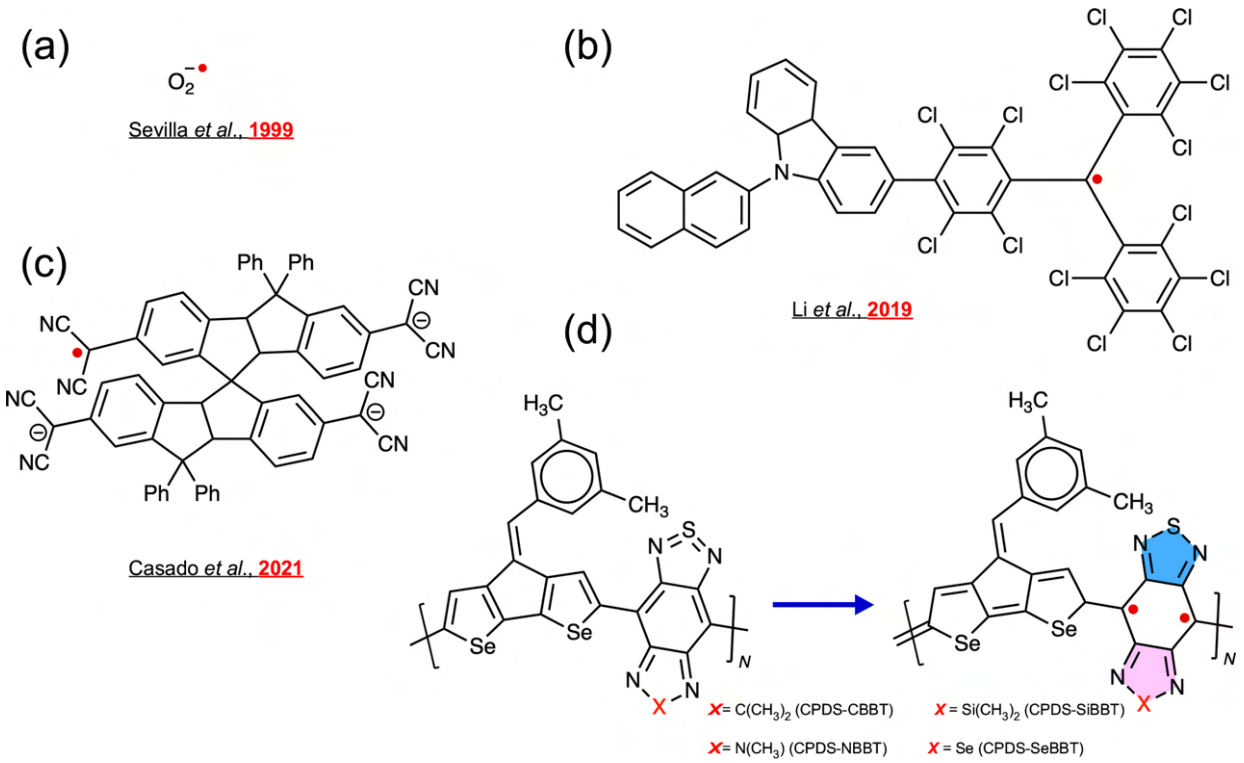

Fig. 1 (a–c) Prototypical examples of molecules with non-Aufbau orbital ordering in different charged states. (d) Molecular and resonance structures of the high-spin state ($S = 1$) polymers with a variable spin distribution, where modulation of aromaticity in the auxiliary ring (light purple color) tunes the spin topology and orbital ordering varying from Aufbau to non-Aufbau studied in this work.

energy level inversion.[30–32] Materials with a non-Aufbau orbital ordering are technologically relevant in both conducting and magnetic-based applications.[33] Interestingly, the SOMO–HOMO energy level inversion is only reported in radical species,[26,30–39] and recently been observed in cyclic carbenes.[40] One-electron oxidation of these species produces a high-spin triplet ground-state. However, the intrinsic non-Aufbau orbital ordering is not reported for open-shell high-spin ground-state polymers in the neutral state.

We report D−A conjugated polymers comprising of donor unit cyclopentadiselenophene (CPDS) and different non(semi)-metallic elements (C, Si, N, and Se) substituted benzobis[1,2-c;4,5-c′]bis[1,2,5]thiadiazole (BBT) acceptor, CBBT, SiBBT, NBBT, and SeBBT, respectively (Fig. 1d). The ease of tunability in the molecular topology of D−A polymers provide an opportunity in tailoring their properties and facilitate a broad range of applicability.[4,23,41–45] We employed the atomistic engineering technique by replacing the sulfur atom in one of the thiadiazole units of the BBT acceptor by C, Si, N, and Se, respectively, which enabled tuning their orbital topologies. Significant amounts of works have been conducted based on the idea of atomistic engineering, which is almost exclusively focused on tuning the molecular band gap so as to have red-shifted absorption into the solar spectrum.[46–58] However, a thorough study delineating the effect of heteroatoms on the spin topology of high-spin ground-state molecules is not available in the literature.

2 Computational details

Geometry optimizations are performed with Gaussian 16 software package[59] without any symmetry constraints. Molecular geometries for the electronic singlet ($S = 0$) and the triplet ($S = 1$) states of the model oligomers ($N = 1$ to 8) are optimized using hybrid density functional, B3LYP.[60,61] For the Si and Se atoms, LANL2DZdp basis set is used along with associated effective core potentials[62,63] and 6-31G(d,p)[64] basis set is used for other atoms. All parameters for geometry optimizations are set to default. UltraFine grids are used for numerical integration (see Table S1 for comparison with other grids). As we can see, increasing the number of grid points does not affect the reported values. For larger oligomers, geometries are considered optimized once the forces on all atoms converged to zero.[65] Unless otherwise specified, analyses are performed with (U)B3LYP level of theory. Full computational details can be found in these references.[9,20]

We have performed a dihedral scan along the connecting bond of the donor unit and the acceptor unit of a monomer to identify the lowest energy conformer (see Fig. S1). Therefore, all polymers considered in the present work are arranged according to their minimum energy conformations. Our previous work shows that the minimum energy configuration connects the olefin unit to the donor in an alternating arrangement.[20] As a result, we arranged the thiadiazole units in an alternating manner. We have also performed calculations on a dimer by arranging all the thiadiazole units on the same side and compared the stability of these two configurations with the singlet-triplet energy gap (see Table

S2). As we can see, arranging the thiadiazole units in an alternating manner results in more stable configuration than arranging all the thiadiazole units in the same direction, except for the CPDS-SeBBT, where both configurations are equally likely. However, as we are taking a difference between the energies of the singlet and triplet states, the differences in singlet–triplet energy gap (ΔE_{ST}) are minimal.

A broken-symmetry (BS)[66] wave function is used to optimize and characterize the open-shell singlet state. As spin contamination is a potential issue, we report the expectation value of the total spin-squared operator in the Supplementary Information (Table S1) for Hartree-Fock (HF) and B3LYP methods. Compared to the HF, B3LYP provides the expectation values close to 1, which is the expected value for the broken symmetry approach that admixes singlet and triplet states.[1] The triplet state is optimized with an unrestricted wave function. The location of the unpaired spins are predicted with NBO7 program package[67]. Isotropic nucleus independent chemical shift ($NICS_{iso}(1)$)[68] is computed with gauge-independent atomic orbital (GIAO)[69] at 1 Å above rings plane, where a large negative $NICS_{iso}(1)$ is an indication of an aromatic structure. Anisotropy of the induced current density (ACID) method[70] at CSGT-UB3LYP/6-31G(d,p) level of theory[71] is used to generate the ring current density and rendering is performed with a locally developed code. The 2D-ICSS (2D-isochemical shielding surface) maps are generated by the method developed by Klod *et al.*[72] The harmonic oscillator model of aromaticity (HOMA)[73] is calculated with:

$$HOMA = 1 - \frac{98.89}{n}\sum_{i=1}^{n}(R_i - 1.397)^2 \quad (1)$$

where, n is the number of bonds considered in a particular ring, R_i is the optimized bond length at the equilibrium geometry. HOMA $= 1$ indicates an aromatic structure.[73,74] The optimally tuned range-separated hybrid functional (OT-RSH) calculations are performed with LC-ωHPBE functional[75], where the range-separated parameter, ω is determined by the ionization potential (IP)-scheme[76]. Molecular orbital diagrams and spin density plots are generated with VMD.[77]

3 Results and Discussion

3.1 Selection of donor, acceptor units, and different heteroatoms

We have selected the C-bridged cyclopentadiselenophene (CPDS) as a donor unit, which can increase the π-conjugation, elevate the highest occupied molecular orbital (HOMO), induce a more planar molecular backbone, and can increase the quinoidal character by decreasing the orbital overlap with the π-system due to a large C$-$Se bond in the donor unit.[9,49] The BBT acceptor, on the other hand, has a large electron affinity and a lower lowest unoccupied MO (LUMO), which can reduce the HOMO–LUMO energy gap.[3] A smaller energy gap facilitates the admixing of the frontier MOs (FMOs) into the ground-state, generating open-shell character.[3,9,78–80] The selection of heteroatoms from different groups facilitates assessing the effect of various elements in the periodic table, whereas, previous studies mainly focused on atomistic substitution based on one particular group elements.[46,81] Substitution of different heteroatoms into the thiadiazole unit of the BBT acceptor changes the hybridization of the particular atoms and changes the aromatic character of the thiadiazole unit. The C and Si atoms are sp^3 hybridized, which reduces the aromatic character of the thiadiazole unit. On the other hand, the N atom is sp^2 hybridized, substitution of N atom increases the aromatic character of the thiadiazole unit. Therefore, changing the hybridization of the heteroatoms modulates the bond length alternation (BLA) in the thiadiazole units, hence significantly changing the local aromatic/quinoidal character[46,48,49] of the BBT acceptor; therefore, a distinct change in the electronic properties and spin topologies is observed. A highly quinoidal molecular backbone can increase the open-shell character and reduce the singlet–triplet energy gap (ΔE_{ST}).[9,48] Furthermore, the heteroatom (C, Si, and N) inclusion facilitates the addition of more solubilizing $-CH_3$ groups, which not only will increase the solubility in conventional solvents but also will kinetically block the reactive sites, increasing the stability of the polymers.[4,19,23]

3.2 Effect of different heteroatoms on the orbital ordering

We have extensively analysed the molecular orbitals (MOs) along with their energies to gain insights into the nature of SOMO–HOMO energy level inversion in these different polymers and establish a design paradigm. This can facilitate designing novel materials with intriguing orbital ordering in the neutral state. Interestingly, the orbital ordering is exclusively modulated by the different atomistic substitutions. Such as the C, Si, and Se atoms substituted polymers show a non-Aufbau orbital ordering. However, the orbitals are ordered according to the increased energy in the N substituted CPDS-NBBT polymer (See Fig. S2–S21), following Aufbau principle.

In the case of a smaller repeat unit ($N = 2$) for the C substituted polymer (Fig. S2), spin-orbital 235α (α-SOMO) is higher in energy and localized at one end of the π-conjugated backbone. Therefore, it constitutes one of the unpaired electrons in the diradical polymer. The β spins are mostly delocalized along the polymer backbone. However, the frontier spin-orbital 235β (β-SOMO) has the same spatial distribution and energy with the 234α (α-SOMO-1) spin-orbital, making these two orbitals resembled as a closed-shell configuration (i.e, a HOMO). Therefore, the 234β (β-SOMO-1) spin-orbital acts as another unpaired electron, which indicates the non-Aufbau orbital ordering is visible even in the smallest repeat unit of the C substituted polymer. Looking at the spatial orientations and energies of the MOs, there are four unpaired electrons in the CPDS-CBBT dimer (Fig. S2). However, there is no polyradical character observed in the studied polymers (Table S3), which is also been reported for other BBT-based materials.[8,78] This is probably due to the fact that the unpaired electrons which are deeper in energy do not contribute to the open-shell character, limiting the open-shell character to diradical (see Table S3). A similar phenomenon in orbital orientation is observed for the Si substituted polymer as well (Fig. S6). However, in the case of smaller units ($N = 2$) of N and Se substituted polymers, normal Aufbau orbital ordering is observed (Fig. S10

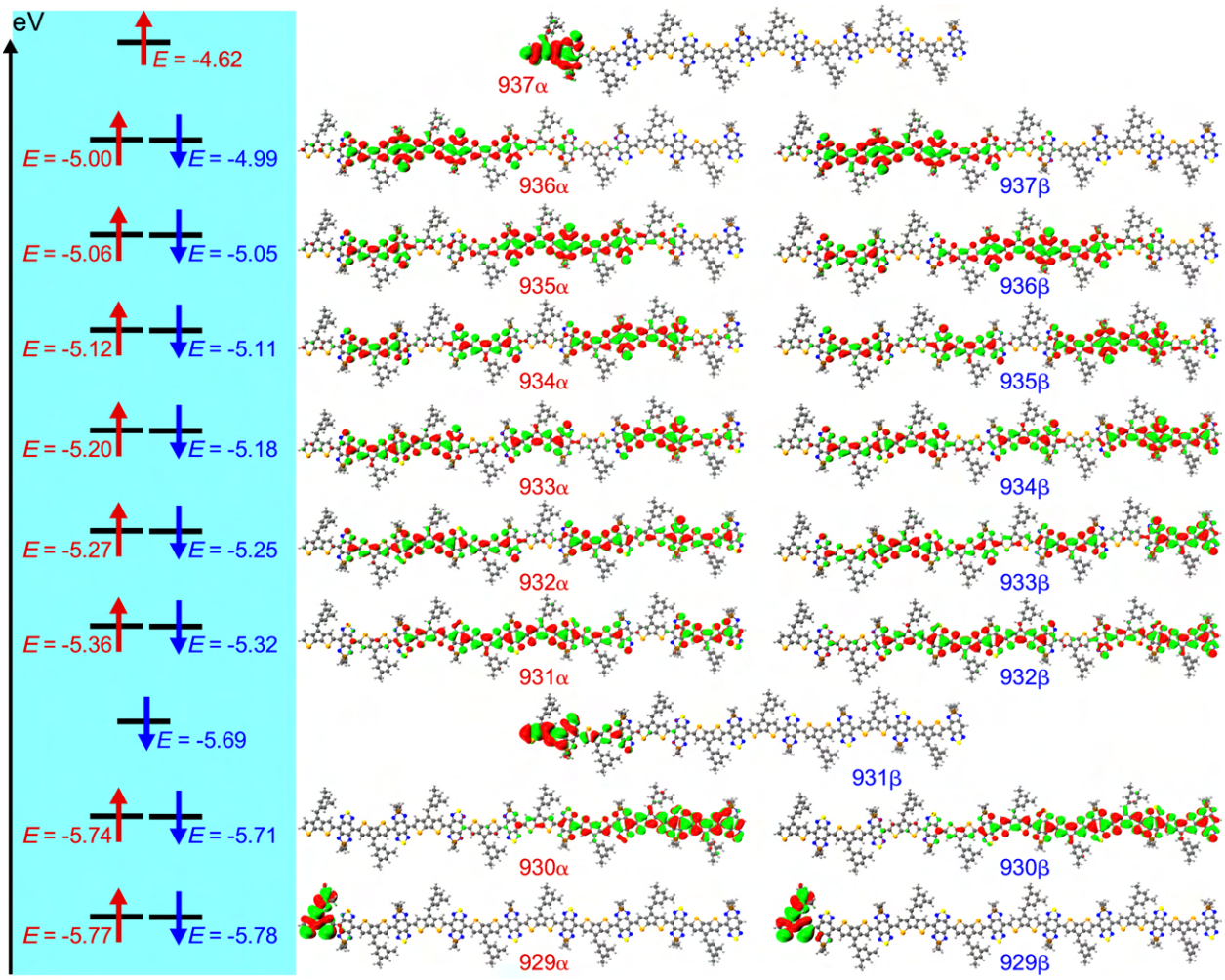

Fig. 2 Molecular orbitals (MOs) and their energies at the singlet ($S = 0$) state for CPDS-SiBBT octamer ($N = 8$). The green and red surfaces represent positive and negative contributions of the MOs at an isovalue = 0.01 au.

and S14).

Increasing the oligomer chain length ($N = 4$–8) downshifts the unpaired β spin for C, Si, and Se substituted polymers. Such as in the case of the CPDS-SiBBT tetramer ($N = 4$), spin orbital 466β (β-SOMO−3) is out of phase with the frontier α-SOMO (Fig. S7). However, for the octamer ($N = 8$), β-SOMO−6 (931β) is similar in orbital pattern with the α-SOMO (Fig. 2). Due to a large Coulomb repulsion in placing an unpaired electron into the spatially delocalized SOMO's, the β-spin is pushed downward in energy, providing a non-Aufbau orbital orientation.[17] We have also analysed the orbital orientations and energies of CPDS-SiBBT tetramer ($N = 4$) with BLYP[60], CAM-B3LYP,[82] ωB97X-D,[83] and OT-RSH (LC-ωHPBE($\omega = 0.90$)) methods. These functionals also provide a non-Aufbau orbital configuration (Fig. S18–S21), which indicates the non-Aufbau orbital orientation is an intrinsic property of the CPDS-SiBBT polymer. On the other hand, the α-SOMO and β-SOMO of the CPDS-NBBT octamer have different spatial orientations and energies, which indicates these two spin-orbitals constitutes the frontier molecular orbitals (Fig. S13). As a result, the orbital orientation follows the normal Aufbau principle according to the increasing in energy. This indicates the orbital arrangement is modulated by different atomistic substitution, which is observed even in the smallest repeat units. Interestingly, when an asymmetric arrangement is considered for the polymers, such as end-capping with donor or acceptor units, we observed two different scenarios. When the CPDS-SiBBT heptamer ($N = 7$) is end-capped with acceptor units, the two spin-orbital α-SOMO−7 (864α) and β-SOMO−13 (861β) are higher in energy than the HOMOs (Fig. S22). This indicates the CPDS-SiBBT polymer when end-capped with the BBT acceptor show non-Aufbau orbital ordering. However, when the polymer is end-capped with donor units, the frontier α-SOMO (886α) and β-SOMO (886β) is arranged according to the Aufbau principle (Fig. S23). Therefore, the Aufbau and non-Aufbau orbital ordering is also being modulated with different end groups in the CPDS-SiBBT polymer.

The driving force for this unique orbital orientation is originating due to the different atoms substituted into the thiadiazole unit of the BBT acceptor. This is due to the fact that the heteroatom substitutions modulate the local aromatic character of the thiadiazole units, which alters the aromatic/quinoidal character along the polymer's backbones. We have analysed the bond lengths

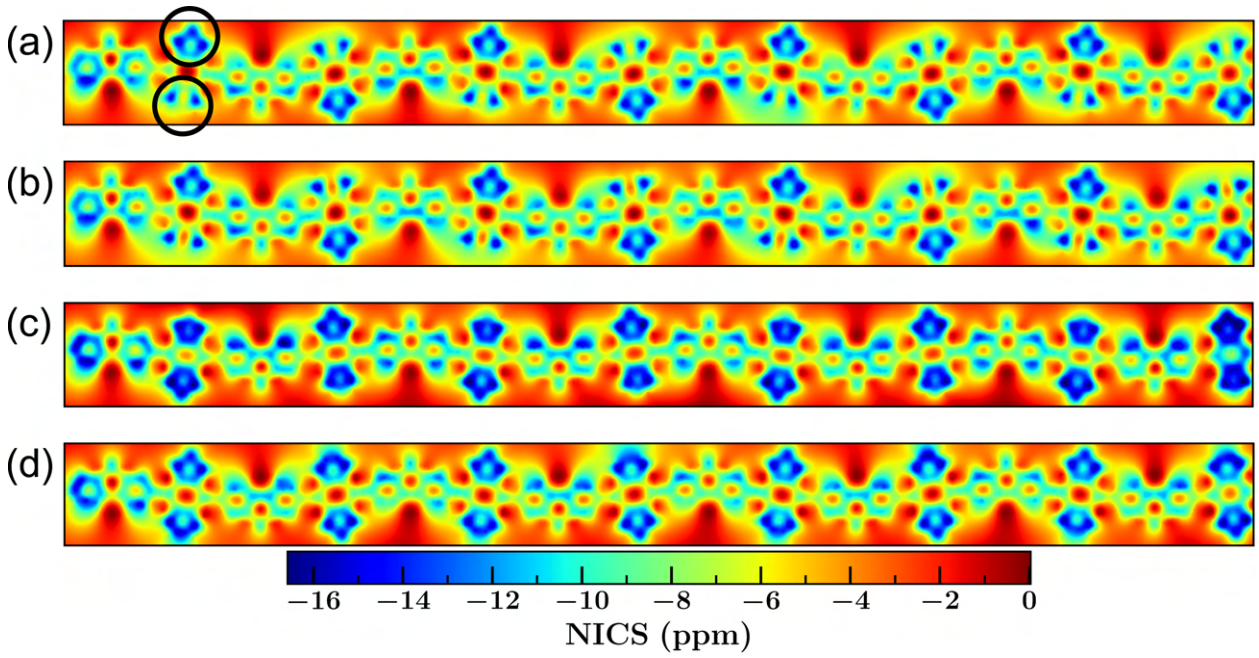

Fig. 3 Calculated 2D-ICSS maps for the (a) CPDS-CBBT, (b) CPDS-SiBBT, (c) CPDS-NBBT, and (d) CPDS-SeBBT polymers ($N = 8$) in the triplet ($S = 1$) state. The change in the aromatic character of the substituted and unsubstituted thiadiazole units for the CPDS-CBBT are highlighted with the black open circles.

of the substituted BBT acceptor unit and performed $NICS_{iso}(1)$ and 2D-ICSS calculations to assess the aromatic character. Bond length analysis indicates substitution of different heteroatoms significantly alters the bond lengths of the thiadiazole unit. The N−S bond of the unsubstituted thiadiazole unit in the singlet state ($S = 0$) is ≈ 1.65 Å, whereas, the N−X (X = C, Si, N, and Se) bond varies as 1.47–1.48, 1.77–1.78, 1.32–1.33, and 1.81–1.82 Å, in the CPDS-CBBT, CPDS-SiBBT, CPDS-NBBT, and CPDS-SeBBT polymers ($N = 8$), respectively (see Table S4–S7). The largest N−X bond is observed in the Se substituted thiadiazole unit due to a larger atomic size of the Se atom and the smallest N−X bond is predicted in the CPDS-NBBT polymer. As a result, the Se substituted thiadiazole unit should show the least aromatic character and the N substituted thiadiazole unit provides the strongest aromaticity.[48] The C−N (L1 and L4 in Table S4–S7) bonds of the unsubstituted thiadiazole unit is ≈ 1.33 Å, which is close to a double-bond. In the case of the C and Si substituted polymers, the C−N (L5 and L8 in Table S4–S5) bond is more reduced (≈ 1.30 Å), increasing the double-bond, and hence the quinoidal character of the substituted thiadiazole unit. The largest C−N (L5 and L8 in Table S6) bond (≈ 1.35 Å) is observed for the N substituted polymer, which is also close to the N−N bond (L6 and L7 in Table S6). Therefore, the N substitution equalizes the bond lengths in the thiadiazole unit of the CPDS-NBBT polymer, increasing the aromatic character of the polymer backbone.

This is been reflected in the observed $NICS_{iso}(1)$ values as well (see Table S8–S23). The largest (more negative) calculated $NICS_{iso}(1)$ value is observed for the N substituted thiadiazole unit (ring 8D) (≈ −12.50 ppm), whereas, the smallest (less negative) $NICS_{iso}(1)$ value is observed for the CPDS-SiBBT polymer (ring 8F) (≈ −2.90 ppm) (Table S15 and S19). Although the N substituted thiadiazole unit provides a large aromatic character due to a smaller N−N bond, the largest N−Se bond containing thiadiazole unit (8F) does not show the least aromatic character ($NICS_{iso}(1)$ ≈ −9.88 ppm) (Table S23). In the open-shell form, the hypervalent Se atom goes from high-energy N=Se=N to N-Se-N configuration by recovering aromatic stabilization energy in the thiadiazole unit, which facilitates achieving a high open-shell diradical character in the CPDS-SeBBT polymer.[20] The 2D-ICSS maps indicate both the thiadiazole units of the CPDS-SeBBT polymer are magnetically shielded (negative 2D-ICSS: aromatic) (Fig. 3). On the other hand, the thiadiazole unit with the substituted heteroatoms in the CPDS-CBBT and CPDS-SiBBT polymers are magnetically de-shielded (less negative 2D-ICSS: quinoidal), and the unsubstituted thiadiazole unit is magnetically shielded (Fig. 3). Therefore, although, the Se substituted polymer has the largest N−Se bond, however; the bond polarization is largest in the case of the Si substituted polymer due to a large difference in the element's electronegativity.[48] Also, due to a change in the elements hybridization, the aromatic/quinoidal character changes in the thiadiazole units of the BBT acceptor, which modulates the orbital ordering of the studied polymers.

3.3 Effect of different heteroatoms on the spin density distribution

Modulation of the spin density distribution controls the ground-state electronic and magnetic properties.[5,20] We have analysed the spin density distribution along with the spin values as a function of oligomer chain lengths (see Fig. S24–S48). As can be seen from Fig. 4, except for the CPDS-NBBT polymer, all the polymers significantly localize the spin densities at the two opposite ends, as observed in the BBT-based polymers.[20] The most

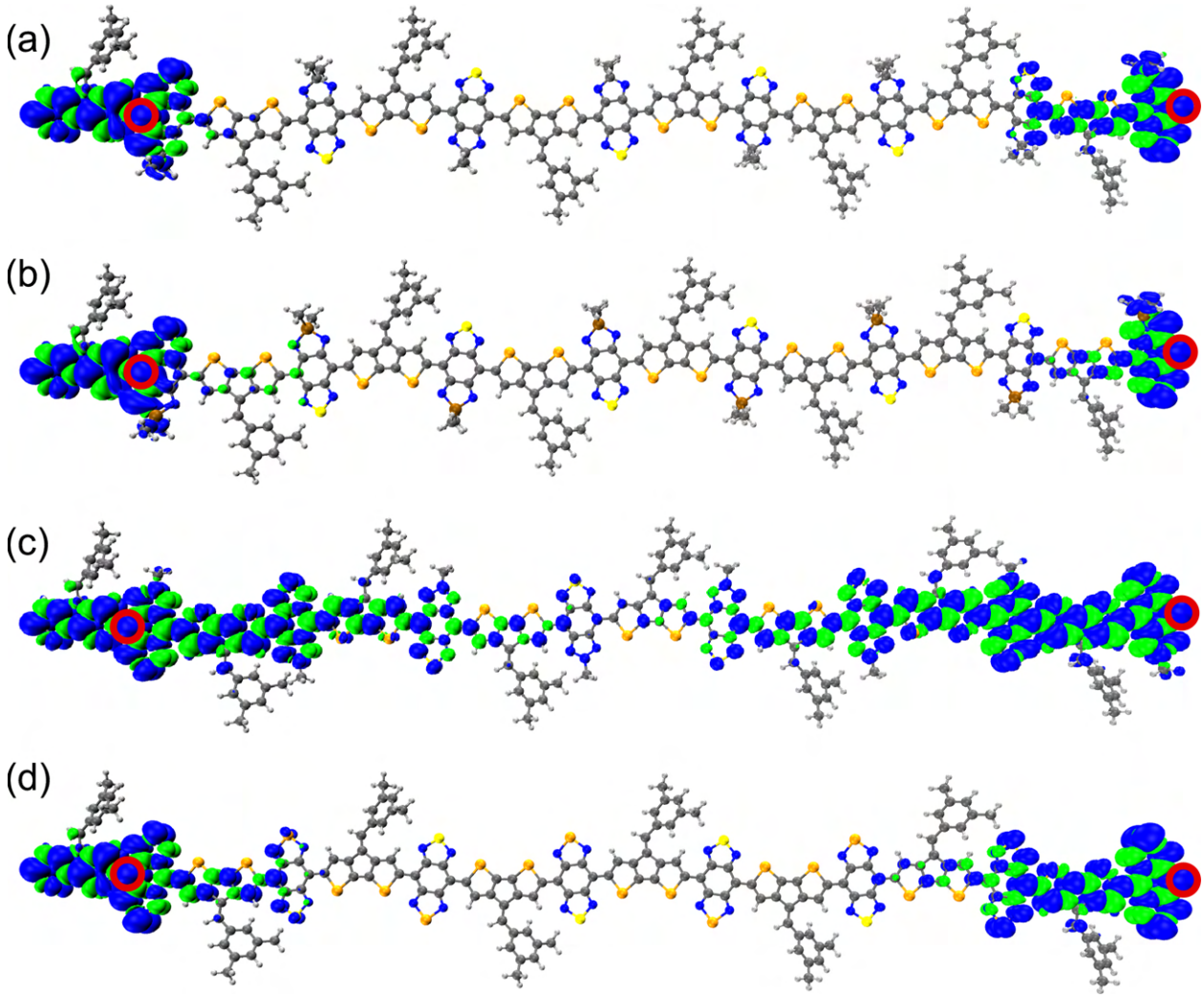

Fig. 4 The optimized ground-state geometries and observed spin density distributions for the BBT-derivatives, (a) CPDS-CBBT, (b) CPDS-SiBBT, (c) CPDS-NBBT, and (d) CPDS-SeBBT ($N = 8$) polymers in their triplet ($S = 1$) state. The blue and green surfaces represent positive and negative contributions of the spin density at an isovalue = 0.0002 au. The most probable locations of the unpaired electrons are highlighted with open circles.

spin localization is achieved in the CPDS-SiBBT polymer than the other polymers, where spin localization is visible from the dimer ($N = 2$) (see Fig. S46). Increasing the oligomer chain lengths further localizes the unpaired electrons at the two opposite ends of the C, Si, and Se substituted polymers than the N substituted polymer due to the delocalized nature of the sp^2 hybridized N atom (Fig. 4, S46–S48), which indicates the atomistic substitution modulates the spin density in the studied polymers.

Analysing the MOs and spin density distribution, we observe a disparity between the SOMOs and spin density distribution for the CPDS-CBBT, CPDS-SiBBT, and CPDS-SeBBT polymers, which have a non-Aufbau orbital ordering. Such as the SOMOs of the C, Si, and Se substituted polymers located on the same side of the polymers, whereas, the spin density is localized at the two opposite ends (Fig. S24–S45). Therefore, the SOMOs have a very small contributions in the spin density for the C, Si, and Se polymers than the N substituted polymer. Accumulation of the fractional contributions from the MOs probably leading to an end localized spin density distribution on the C, Si, and Se substituted polymers.

Variation of the aromatic character along the polymer backbone facilitates spin separation in the BBT-based materials.[20] To rationalize the different spin density distributions, we have analysed the aromatic/quinoidal character with bond lengths along the polymer's backbones. The calculated bond lengths along the conjugated path (Fig. 5, Table S24–S27) in the benzenoid ring of the BBT core vary within 1.413–1.493, 1.418–1.546, 1.398–1.448, and 1.409–1.460 Å, in the CPDS-CBBT, CPDS-SiBBT, CPDS-NBBT, and CPDS-SeBBT polymers, respectively. This indicates the bond length alternation (BLA) is largest in the CPDS-SiBBT polymer, whereas BLA is significantly reduced in the N substituted polymer. Therefore, the CPDS-SiBBT polymer has the most quinoidal backbone compared to the other polymers. As a result, the Si substituted polymer has the most localized spin density distribution and spins are significantly polarized than the other polymers. On the other hand, the CPDS-NBBT polymer show almost delocalized spin distribution along the whole backbone. The calculated spin values are largest at the two opposite ends of the polymers, and

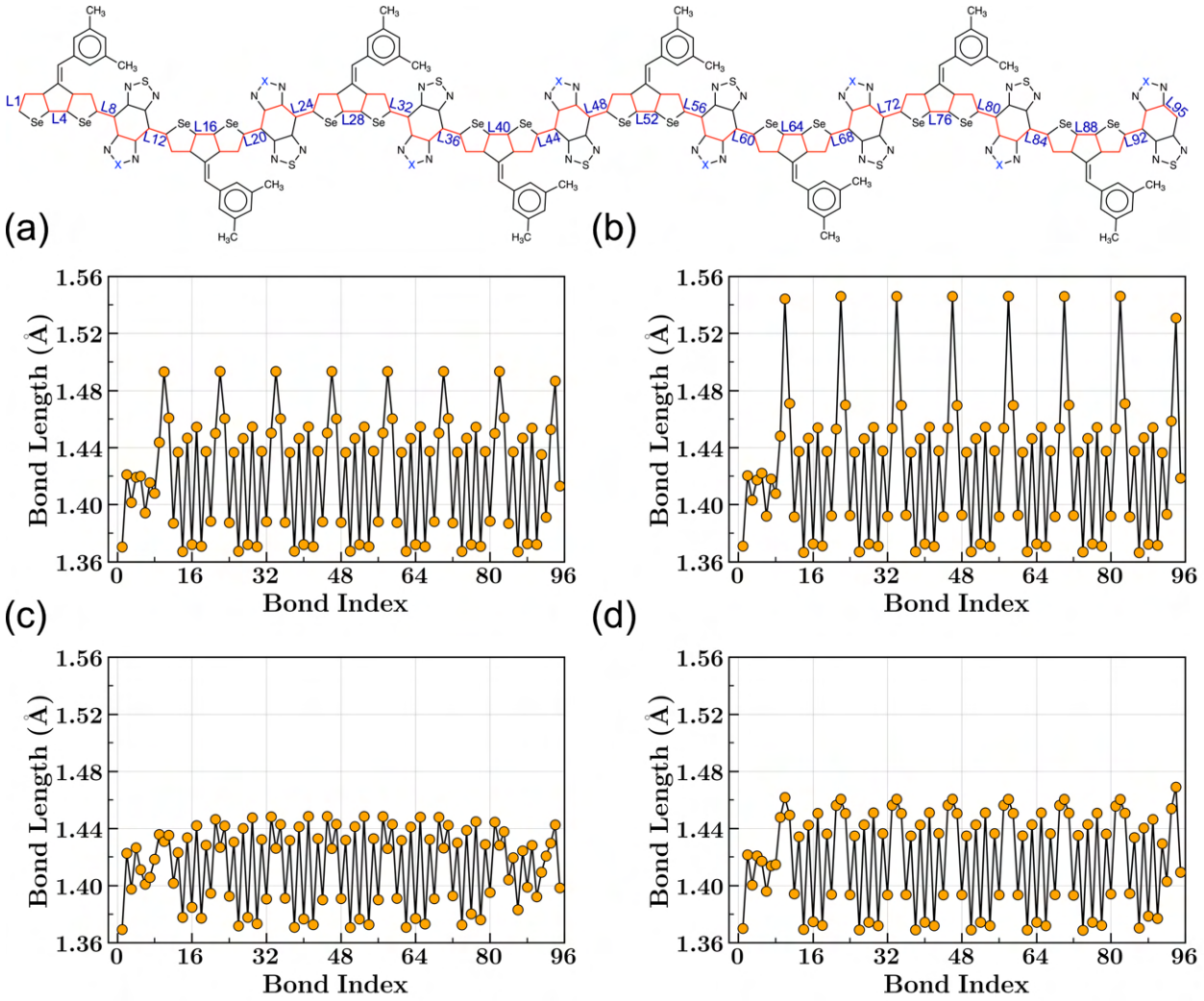

Fig. 5 The calculated bond lengths of the (a) CPDS-CBBT (X = C), (a) CPDS-SiBBT (X = Si), (a) CPDS-NBBT (X = N), and (a) CPDS-SeBBT (X = Se) polymers ($N = 8$) along the highlighted π-conjugated path. Bond lengths computed at UB3LYP/6-31G(d,p) level of theory and basis set are provided for the triplet ($S = 1$) state. Different atomistic substitution changes the BLA along the conjugation backbone, changing the electronic properties and spin distribution.

the singlet ($S = 0$) and triplet ($S = 1$) states have the same positive values (Fig. S49–S50). Interestingly, the N atom adjacent to the C, Si, and Se heteroatoms shows a very high spin value, whereas, the same N atom has essentially no spin in the CPDS-NBBT polymer. This also indicates the bond polarization is significant in the CPDS-CBBT, CPDS-SiBBT, and CPDS-SeBBT polymers than the CPDS-NBBT polymer. These highly spin-polarized polymers can be used as a building block for spintronic devices.[33]

Increasing the oligomer chain length increases the quinoidal character at the core of the polymers, whereas, both ends become more aromatic (see Table S8–S23). Such as ring 1A of the CPDS-CBBT octamer has a $NICS_{iso}(1)$ value of ≈ -7.06 ppm, whereas ring 4A show a significantly reduced aromatic character (≈ -3.60 ppm) (see Table S11). The benzenoid ring (4E) at the polymer core indicates a very small (less negative) $NICS_{iso}(1)$ value (≈ -0.25 ppm) than the benzenoid ring (8E) at the chain end (≈ -0.96 ppm). Similar phenomena are observed in the CPDS-SiBBT, CPDS-NBBT, and CPDS-SeBBT polymers as well (see Fig. S51). The 2D-ICSS maps also show increased magnetic shielding at both end units, indicating increased aromatic character (Fig. 3). Therefore, the spins are separated from the large quinoidal core to the more stable aromatic ends, localizing spins to the two opposite ends of the polymers (Fig. 4 and S46–S48).

3.4 Effect of different heteroatoms on the singlet–triplet energy gap (ΔE_{ST})

The characteristic features of the open-shell materials are best described with the energy difference between the ground-state and lowest excited-state, and open-shell character.[1] All the calculated electronic properties for the polymers are provided in Table 1 and Table S3. The trend in the calculated singlet–triplet energy gap (ΔE_{ST}) provides insights into the addition of different heteroatoms and the oligomer chain lengths. The observed ΔE_{ST} and open-shell character are entirely dependent on the different heteroatoms substituted into the thiadiazole unit of the BBT acceptor.

Table 1 Computed electronic properties at (U)B3LYP/6-31G(d,p) level of theory and basis set for the CPDS-CBBT, CPDS-SiBBT, CPDS-NBBT, and CPDS-SeBBT polymers as a function of chain length (N). The singlet–triplet energy gap ($\Delta E_{ST} = E_S - E_T$), population ($P_T$) of the triplet ($S = 1$) state at room temperature, energies of the highest occupied MO (HOMO) and the lowest unoccupied MO (LUMO), energetic difference between the FMOs (E_g), and diradical character index (y_0) of the polymers. Energy values are in eV, and y_0 is a dimensionless quantity.

Polymer	N	ΔE_{ST}	P_T	HOMO	LUMO	E_g	y_0
CPDS-CBBT	2	-5.33×10^{-4}	74.63	−4.64	−3.37	1.27	0.974
	4	$+2.72 \times 10^{-7}$	75.00	−4.58	−3.41	1.17	1.000
	6	0.00×10^{-0}	75.00	−4.57	−3.42	1.15	1.000
	8	0.00×10^{-0}	75.00	−4.57	−3.43	1.14	1.000
CPDS-SiBBT	2	$+3.90 \times 10^{-4}$	75.27	−4.69	−3.49	1.20	0.999
	4	0.00×10^{-0}	75.00	−4.64	−3.53	1.11	1.000
	6	0.00×10^{-0}	75.00	−4.63	−3.54	1.08	1.000
	8	0.00×10^{-0}	75.00	−4.62	−3.55	1.07	1.000
CPDS-NBBT	2	-2.13×10^{-1}	0.12	−4.35	−3.11	1.24	0.193
	4	-2.78×10^{-2}	51.93	−4.15	−3.19	0.96	0.838
	6	-4.01×10^{-3}	72.14	−4.09	−3.22	0.87	0.977
	8	-5.82×10^{-4}	74.60	−4.07	−3.23	0.85	0.997
CPDS-SeBBT	2	-1.86×10^{-2}	60.27	−4.60	−3.45	1.16	0.832
	4	-5.88×10^{-5}	74.96	−4.49	−3.48	1.00	0.995
	6	0.00×10^{-0}	75.00	−4.46	−3.49	0.97	1.000
	8	0.00×10^{-0}	75.00	−4.45	−3.50	0.95	1.000

The effect of substituting different heteroatoms on the acceptor unit is visible at a smaller oligomer unit from the calculated ΔE_{ST} and diradical character (y_0). At the monomer unit ($N = 1$), ΔE_{ST} for the Se substituted polymer (CPDS-SeBBT) is 0.114 eV smaller (Table S3) than our previously reported CPDS-BBT polymer.[9] This indicates, in a same group of the periodic table, increasing the atomic size and a reduction in the electronegativity should reduce the singlet–triplet energy gap. Also, a similar phenomenon is observed for the C and Si substituted polymers, CPDS-CBBT and CPDS-SiBBT, receptively, where a larger atom with reduced electronegativity reduces the ΔE_{ST} and increases open-shell diradical character. However, this directly contradicts the recent findings from Wu *et al.*, where it is reported that increasing the heteroatomic sizes increases the ΔE_{ST} and reduces diradical character.[81] On the other hand, the N substituted polymer CPDS-NBBT show a closed-shell ($y_0 = 0$) structure with the largest calculated ΔE_{ST} (0.657 eV at $N = 1$) among the studied polymers (see Table S3). This indicates atomistic substitution can modulate the electronic properties of the studied polymers.

Increasing the oligomer length reduces the ΔE_{ST} gap, as observed from previous studies.[9,19,20] Except the CPDS-NBBT polymer, the CPDS-CBBT, CPDS-SiBBT, and CPDS-SeBBT polymers show a large diradical character even at the monomer ($N = 1$) unit (see Table S3), which indicates the open-shell form is more stable in energy than the closed-shell configuration. This is visible from the energy diagram (Fig. S52), where the closed-shell state of CPDS-CBBT dimer ($N = 2$) is 15.4 kcal/mol above the reference singlet open-shell state. Comparing the energy difference between the open-shell and closed-shell state in the smaller repeat unit, the largest value is obtained for the CPDS-SiBBT dimer (17.3 kcal/mol), indicating a larger diradical character in a smaller repeat unit. However, the closed-shell configuration of CPDS-NBBT dimer is close to a degenerate state with its open-shell configuration, showing a very small diradical character for this polymer in the smaller repeat unit. As the number of repeat units are increased, a rapid decrease in the ΔE_{ST} gap is observed for the C, Si, and Se substituted polymers than the N substituted polymer. The Se substituted polymer shows a degenerate ΔE_{ST} gap at $N = 6$ repeat unit, whereas, the N substituted polymer has a large ΔE_{ST} gap even at $N = 8$ (Table 1 and S3). Extrapolation of the computed ΔE_{ST} gap with the number of repeat units indicates an inflection point is achieved at $N = 9$ (Fig. S53), which indicates the CPDS-NBBT has a high-spin triplet ($S = 1$) ground-state at a larger repeat unit. In the case of the C substituted polymer CPDS-CBBT, a triplet ($S = 1$) ground-state is observed at $N = 3$, whereas, the dimer ($N = 2$) of CPDS-SiBBT show a triplet ground-state (Table 1 and S3). However, the larger oligomers of CPDS-CBBT, CPDS-SiBBT, and CPDS-SeBBT show a degenerate energy state between the singlet and triplet states. The thermal population of the triplet state increases as the oligomer units are increased. The CPDS-NBBT polymer has no triplet state population for the monomer ($N = 1$) unit; however, a significant population (55.99 %) is observed for the CPDS-SiBBT at room temperature (Table S3). The dimer of the CPDS-SiBBT polymer surpasses the threshold population of a degenerate state (75.00 %), providing the largest value (75.27 %) among the studied polymers.

A stronger π-conjugation can increase the electronic coherence along the polymer backbone.[9] All the polymers possess small dihedral angles between the adjacent donor and acceptor units, which indicates a strong π-conjugation throughout the π framework. The connecting bonds between a donor and adjacent acceptor units in the triplet state ($S = 1$) varies within 1.387–1.408, 1.391–1.408, 1.390–1.420, and 1.393–1.415 Å, for the CPDS-CBBT, CPDS-SiBBT, CPDS-NBBT, and CPDS-SeBBT polymers, respectively (Fig. 5, Table S24–S27). This indicates the C and Si substituted polymers have a larger π-conjugation than the N and Se substituted polymers, least conjugation is observed for the N substituted CPDS-NBBT polymer. Therefore, the π-conjugation of the CPDS-CBBT, CPDS-SiBBT, CPDS-NBBT, and CPDS-SeBBT polymers are modulated with different atomistic substitutions as well. The addition of more repeat units increases the distance between the unpaired electrons of the polymers (Fig. S54), which reduces

the Coulomb repulsion. As a result, the triplet state ($S = 1$) becomes lower in energy than the singlet ($S = 0$) state at a larger repeat unit, generating a high-spin triplet ground-state.

3.5 Effect of different heteroatoms on the open-shell character

The presence of unpaired electrons in the open-shell OSCs can be quantitatively described by the radical indexes, y_i ($i = 0$–1). The y_0 and y_1 represents diradical and tetraradical character, respectively, where the indexes ranges from $0 \leq y_i \leq 1$. Such as, $y_0 = 0$ indicates a closed-shell structure, and $y_0 = 1$ dictates a pure open-shell diradical character, respectively.[84–86] The calculated diradical character provided in the Table 1 and in the Supporting Information (see Table S3) as a function of chain lengths. It is clear from the calculated diradical character that increasing the oligomer chain length increases the y_0, as observed in other studies.[19,20] Although the analysis of MOs indicates the presence of more than two unpaired electrons in these polymers; however, the calculated tetraradical character is very low ($y_1 < 0.10$).

Different atomistic substitutions provide variable open-shell diradical character, which is evident in the smaller repeat units. Such as the Si substituted polymer CPDS-SiBBT show a very high open-shell character ($y_0 = 0.787$) even at the monomer ($N = 1$) unit. However, the N substituted polymer CPDS-NBBT shows a closed-shell configuration ($y_0 = 0.0$) (see Table S3). The dimer of the CPDS-NBBT shows a very small diradical character ($y_0 = 0.193$), which indicates the open-shell and closed-shell configurations are degenerate in energy (Fig. S52). Whereas the Se substituted polymer shows moderate open-shell character for the smaller repeat units, the open-shell character quickly approaches the bond dissociation limit ($y_0 = 1.0$) for C and Si substituted polymers (Table 1 and S3, Fig. S55). This indicates the preferences for a high-spin triplet ($S = 1$) ground-state is largest in the Si and C substituted polymers, and least in the CPDS-NBBT polymer. This is readily visible from the calculated ΔE_{ST} gap as well, where the ΔE_{ST} gap is very high even at the octamer ($N = 8$) of the N substituted polymer; however, the CPDS-CBBT, CPDS-SiBBT, and CPDS-SeBBT polymers show a degenerate ΔE_{ST} gap at the larger repeat units with a significant population of the triplet state at room temperature (see Table 1 and S3). Also, the addition of more repeat units gradually reduces the HOMO–LUMO energy gap (Table 1 and S3, Fig. S56). A small energy gap facilitates admixing of the FMOs into the ground-state, developing open-shell diradical character.

The thiadiazole units of the BBT acceptor recover aromatic stabilization energy in the open-shell configuration, as observed in the previous studies.[20,78] However, the substitution of different heteroatoms significantly alters the local aromatic character of the thiadiazole units. For example, the calculated $NICS_{iso}(1)$ value of the CPDS-BBT ($N = 8$)[20] unsubstituted thiadiazole unit in the singlet state ($S = 0$) is ≈ -9.8 ppm, which indicates a large local aromatic character compared to the six-member benzenoid ring (≈ -1.1 ppm). The corresponding $NICS_{iso}(1)$ value changes according to the substituted heteroatoms, smallest value (less negative) is observed in the Si substituted CPDS-SiBBT polymer ($N = 8$) (≈ -2.82 ppm for the 4F unit) (Table S15) and largest values (more negative) is observed in the N substituted CPDS-NBBT polymer ($N = 8$) (≈ -11.32 ppm for the 4D unit) (Table S19). This indicates insertion of the Si atom reduces the aromatic character and increases the quinoidal character in the thiadiazole unit, which increases the diradical character. However, the N substitution imparts more aromatic character in the CPDS-NBBT polymer backbone, reducing the diradical character. The C and Se substituted polymers show similar reduced aromatic character in the thiadiazole units (-5.45 and -9.31 ppm, respectively); however, the observed $NICS_{iso}(1)$ is significantly larger (more negative) than the Si substituted polymer.

Substitution of different heteroatoms affects the aromatic/quinoidal character of the polymer's backbones, which consequently modulates the open-shell character and orbital topology. Analysis of BLA along the conjugated backbone indicates the dimer ($N = 2$) shows a very small BLA compared to the larger repeat unit (Fig. S57–S72). Different atomistic substitutions provide a different BLA, the largest BLA is observed for the Si substituted polymer, whereas the BLA is significantly reduced for the N substituted polymer. This indicates the CPDS-SiBBT possesses the largest open-shell diradical character than the other polymers, which is observed in the calculated diradical index (Table 1 and S3). In the case of CPDS-SiBBT, the calculated $NICS_{iso}(1)$ value for the benzenoid rings are positive (Table S12–S15, Fig. S51), which indicates the backbone of the CPDS-SiBBT polymer is more quinoidal than the other polymers, which is also been reflected in the observed BLA value. The calculated HOMA values show the CPDS-SiBBT polymer has the smallest HOMA values (less aromatic), and a larger value (more aromatic) is observed for the CPDS-NBBT polymer (Fig. S73), which in line with the $NICS_{iso}(1)$ and BLA calculations. The ACID plots show the thiadiazole units of the CPDS-NBBT and CPDS-SeBBT polymers have two clear clockwise (diatropic) ring currents, which indicates large local aromaticity (Fig. 6). On the other hand, the heteroatoms substituted thiadiazole units of the CPDS-CBBT and CPDS-SiBBT polymers show counter-clockwise (paratropic) ring currents, an indication of reduced aromaticity. Although the cores of the CPDS-CBBT, CPDS-SiBBT, and CPDS-SeBBT polymers show counter-clockwise ring currents, clear clockwise ring currents are visible in the CPDS-NBBT polymer core. This also proves a less quinoidal character in the N substituted polymer than the other polymers, which is also validated with BLA, HOMA, $NICS_{iso}(1)$, and 2D-ICSS maps as well. Therefore, the substitution of different heteroatoms on the BBT acceptor modulates the local aromatic character of the thiadiazole unit, which leads to aromatic/quinoidal backbones in these polymers. A large quinoidal character of the CPDS-CBBT, CPDS-SiBBT, and CPDS-SeBBT facilitate developing large open-shell diradical character in a smaller repeat unit than the CPDS-NBBT polymer.

4 Conclusions

In this work we report novel high-spin ground-state donor−acceptor conjugated polymers where the orbital and spin topologies are modulated by different atomistic substitution.

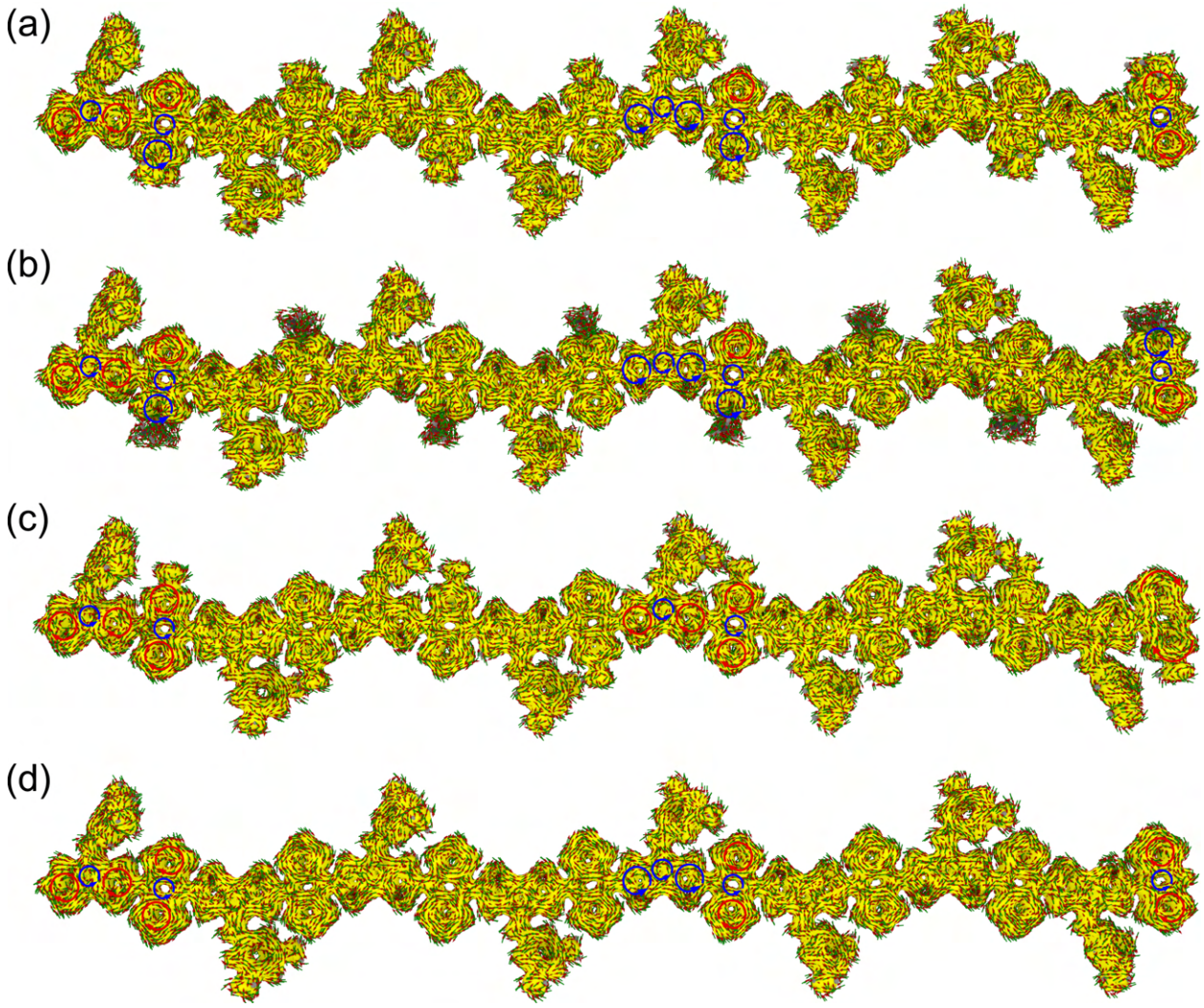

Fig. 6 ACID plots for the (a) CPDS-CBBT, (b) CPDS-SiBBT, (c) CPDS-NBBT, and (d) CPDS-SeBBT polymers ($N = 8$) in the triplet ($S = 1$) state. The clockwise (diatropic: aromatic) and counterclockwise (paratropic: quinoidal) ring currents are indicated by red and blue arrows, respectively. The applied magnetic field is perpendicular to the molecular backbone and pointed out through the molecule plane. ACID plots generated with an isovalue = 0.015 a.u.

We utilized the atomistic engineering to tune the aromatic character in the thiadiazole unit of the BBT acceptor. Substitution of different heteroatoms modulates the aromatic/quinoidal nature of the thiadiazole units, which alters the quinoidal character of the polymer's backbone. As a result, the singlet–triplet energy gap, the energy gap of the FMOs, open-shell diradical character, spin, and orbital topologies are being modulated. The large quinoidal core and aromatic ends accumulate spin densities at the two opposite sides of these polymers. Increasing the oligomer length increases the distance between the unpaired electrons in the polymers' backbone. As a result, the Coulomb repulsion is reduced due to decreased electron–electron repulsions, providing a triplet ground-state at a larger repeat unit. Furthermore, with this simple design strategy, the orbital topologies are modulated from Aufbau to non-Aufbau. The N-substituted CPDS-NBBT polymer with a relatively larger aromatic backbone shows Aufbau orbital ordering. However, the C, Si, and Se substituted polymers with a large quinoidal character show non-Aufbau electronic configurations. These polymers are intriguing synthetic targets for spintronics and room-temperature magnetic materials.

5 Conflicts of interest

There are no conflicts of interest to declare.

6 Acknowledgements

This work is supported by the National Science Foundation (NSF) under grant no. OIA-1757220. The DFT calculations were performed at the high-performance computing center at Mississippi State University. Also, the Extreme Science and Engineering Discovery Environment (XSEDE)[87] was used, which is supported by NSF grant number ACI-1548562. We acknowledge the Texas Advanced Computing Center (TACC) at the University of Texas at Austin for providing (HPC, Stampede 2 (through XSEDE allocation, TG-CHE140141)) resources that have contributed to the research results reported within this paper. We acknowledge helpful discussions with Prof. Steven Gwaltney at Mississippi State Uni-

versity.

Notes and references

1 M. Abe, *Chem. Rev.*, 2013, **113**, 7011–7088.

2 M. Abe, J. Ye and M. Mishima, *Chem. Soc. Rev.*, 2012, **41**, 3808–3820.

3 M. A. Sabuj and N. Rai, *Mol. Syst. Des. Eng.*, 2020, **5**, 1477–1490.

4 K. Wang, L. Huang, N. Eedugurala, S. Zhang, M. A. Sabuj, N. Rai, X. Gu, J. D. Azoulay and T. N. Ng, *Adv. Energy Mater.*, 2019, **9**, 1902806.

5 A. Rajca, *Chem. Rev.*, 1994, **94**, 871–893.

6 S. Wolf, D. Awschalom, R. Buhrman, J. Daughton, v. S. von Molnár, M. Roukes, A. Y. Chtchelkanova and D. Treger, *Science*, 2001, **294**, 1488–1495.

7 L. Bogani and W. Wernsdorfer, *Nanoscience And Technology: A Collection of Reviews from Nature Journals*, World Scientific, 2010, pp. 194–201.

8 M. A. Sabuj, M. M. Huda and N. Rai, *iScience*, 2020, **23**, 101675.

9 M. A. Sabuj, *Organic Open-Shell Materials for Optoelectronic and Magnetic Applications*, Mississippi State University, 2020.

10 A. Rajca, *Adv. Phys. Org. Chem.*, 2005, **40**, 153–199.

11 A. Rajca, M. Takahashi, M. Pink, G. Spagnol and S. Rajca, *J. Am. Chem. Soc.*, 2007, **129**, 10159–10170.

12 N. M. Gallagher, A. Olankitwanit and A. Rajca, *J. Org. Chem.*, 2015, **80**, 1291–1298.

13 N. M. Gallagher, J. J. Bauer, M. Pink, S. Rajca and A. Rajca, *J. Am. Chem. Soc.*, 2016, **138**, 9377–9380.

14 N. Gallagher, H. Zhang, T. Junghoefer, E. Giangrisostomi, R. Ovsyannikov, M. Pink, S. Rajca, M. B. Casu and A. Rajca, *J. Am. Chem. Soc.*, 2019, **141**, 4764–4774.

15 W. Wang, C. Chen, C. Shu, S. Rajca, X. Wang and A. Rajca, *J. Am. Chem. Soc.*, 2018, **140**, 7820–7826.

16 G. J. Snyder, *J. Phys. Chem. A*, 2012, **116**, 5272–5291.

17 A. Rajca, *Nitroxides*, Royal Society of Chemistry, 2021, pp. 359–391.

18 T. Y. Gopalakrishna, W. Zeng, X. Lu and J. Wu, *ChemComm.*, 2018, **54**, 2186–2199.

19 A. E. London, H. Chen, M. Sabuj, J. Tropp, M. Saghayezhian, N. Eedugurala, B. Zhang, Y. Liu, X. Gu, B. Wong, N. Rai and J. Azoulay, *Sci. Adv.*, 2019, **5**, eaav2336.

20 M. A. Sabuj, M. M. Huda, C. S. Sarap and N. Rai, *Materials Advances*, 2021, **2**, 2943–2955.

21 T. L. D. Tam, G. Wu, S. W. Chien, S. F. V. Lim, S.-W. Yang and J. Xu, *ACS Mater. Lett.*, 2020, **2**, 147–152.

22 Z. Zeng, M. Ishida, J. L. Zafra, X. Zhu, Y. M. Sung, N. Bao, R. D. Webster, B. S. Lee, R.-W. Li and W. Zeng, *J. Am. Chem. Soc.*, 2013, **135**, 6363–6371.

23 L. Huang, N. Eedugurala, A. Benasco, S. Zhang, K. S. Mayer, D. J. Adams, B. Fowler, M. M. Lockart, M. Saghayezhian and H. Tahir, *Adv. Funct. Mater.*, 2020, 1909805.

24 P. Karafiloglou, *J. Chem. Educ.*, 1989, **66**, 816.

25 J. Su, W. Fan, P. Mutombo, X. Peng, S. Song, M. Ondracek, P. Golub, J. Brabec, L. Veis and M. Telychko, *Nano Lett.*, 2020, **21**, 861–867.

26 G. Gryn'ova, M. L. Coote and C. Corminboeuf, *WIREs Comput. Mol. Sci.*, 2015, **5**, 440–459.

27 G. Z. Magda, X. Jin, I. Hagymási, P. Vancsó, Z. Osváth, P. Nemes-Incze, C. Hwang, L. P. Biro and L. Tapaszto, *Nature*, 2014, **514**, 608–611.

28 M. Slota, A. Keerthi, W. K. Myers, E. Tretyakov, M. Baumgarten, A. Ardavan, H. Sadeghi, C. J. Lambert, A. Narita and K. Müllen, *Nature*, 2018, **557**, 691–695.

29 V. Morozov and E. Tretyakov, *J. Mol. Model.*, 2019, **25**, 58.

30 M. J. Raiti and M. D. Sevilla, *J. Phys. Chem. A*, 1999, **103**, 1619–1626.

31 H. Guo, Q. Peng, X.-K. Chen, Q. Gu, S. Dong, E. W. Evans, A. J. Gillett, X. Ai, M. Zhang and D. Credgington, *Nat. Mater.*, 2019, **18**, 977–984.

32 S. Medina Rivero, R. Shang, H. Hamada, Q. Yan, H. Tsuji, E. Nakamura and J. Casado, *Bull. Chem. Soc. Jpn.*, 2021, **94**, 989–996.

33 T. Sugawara, H. Komatsu and K. Suzuki, *Chem. Soc. Rev.*, 2011, **40**, 3105–3118.

34 G. Gryn'ova and M. L. Coote, *J. Am. Chem. Soc.*, 2013, **135**, 15392–15403.

35 P. Franchi, E. Mezzina and M. Lucarini, *J. Am. Chem. Soc.*, 2014, **136**, 1250–1252.

36 B. L. Westcott, N. E. Gruhn, L. J. Michelsen and D. L. Lichtenberger, *J. Am. Chem. Soc.*, 2000, **122**, 8083–8084.

37 G. Gryn'ova, D. L. Marshall, S. J. Blanksby and M. L. Coote, *Nat. Chem.*, 2013, **5**, 474–481.

38 Y. Wang, H. Zhang, M. Pink, A. Olankitwanit, S. Rajca and A. Rajca, *J. Am. Chem. Soc.*, 2016, **138**, 7298–7304.

39 S. M. Quintero, J. L. Zafra, K. Yamamoto, Y. Aso, Y. Ie and J. Casado, *J. Mater. Chem. C*, 2021, **9**, 10727–10740.

40 R. Murata, Z. Wang, Y. Miyazawa, I. Antol, S. Yamago and M. Abe, *Org. Lett.*, 2021, **23**, 4955–4959.

41 J. D. Yuen, R. Kumar, D. Zakhidov, J. Seifter, B. Lim, A. J. Heeger and F. Wudl, *Adv. Mater.*, 2011, **23**, 3780–3785.

42 J. D. Yuen, J. Fan, J. Seifter, B. Lim, R. Hufschmid, A. J. Heeger and F. Wudl, *J. Am. Chem. Soc.*, 2011, **133**, 20799–20807.

43 J. Fan, J. D. Yuen, M. Wang, J. Seifter, J.-H. Seo, A. R. Mohebbi, D. Zakhidov, A. Heeger and F. Wudl, *Adv. Mater.*, 2012, **24**, 2186–2190.

44 Y. Zheng and F. Wudl, *J. Mater. Chem. A*, 2014, **2**, 48–57.

45 J. Xiong, N. Eedugurala, Y. Qi, W. Liu, A. R. Benasco, Q. Zhang, S. E. Morgan, M. D. Blanton, J. D. Azoulay and Q. Dai, *Sol. Energy Mater. Sol. Cells*, 2021, **220**, 110862.

46 G. L. Gibson, T. M. McCormick and D. S. Seferos, *J. Am. Chem. Soc.*, 2012, **134**, 539–547.

47 M. Li, L. Kou, L. Diao, Q. Zhang, Z. Li, Q. Wu, W. Lu, D. Pan and Z. Wei, *J. Phys. Chem. C*, 2015, **119**, 9782–9790.

48 R. S. Ashraf, I. Meager, M. Nikolka, M. Kirkus, M. Planells, B. C. Schroeder, S. Holliday, M. Hurhangee, C. B. Nielsen and H. Sirringhaus, *J. Am. Chem. Soc.*, 2015, **137**, 1314–1321.

49 Z. Fei, Y. Han, E. Gann, T. Hodsden, A. S. Chesman, C. R.

McNeill, T. D. Anthopoulos and M. Heeney, *J. Am. Chem. Soc.*, 2017, **139**, 8552–8561.

50 C.-C. Chang, C.-P. Chen, H.-H. Chou, C.-Y. Liao, S.-H. Chan and C.-H. Cheng, *J. Polym. Sci. A Polym. Chem.*, 2013, **51**, 4550–4557.

51 H. A. Saadeh, L. Lu, F. He, J. E. Bullock, W. Wang, B. Carsten and L. Yu, *ACS Macro Lett.*, 2012, **1**, 361–365.

52 Y.-J. Hwang, G. Ren, N. M. Murari and S. A. Jenekhe, *Macromolecules*, 2012, **45**, 9056–9062.

53 C.-H. Tsai, A. Fortney, Y. Qiu, R. R. Gil, D. Yaron, T. Kowalewski and K. J. Noonan, *J. Am. Chem. Soc.*, 2016, **138**, 6798–6804.

54 M. Al-Hashimi, Y. Han, J. Smith, H. S. Bazzi, S. Y. A. Alqaradawi, S. E. Watkins, T. D. Anthopoulos and M. Heeney, *Chem. Sci.*, 2016, **7**, 1093–1099.

55 D. Çakal, A. Cihaner and A. M. Önal, *J. Electroanal. Chem.*, 2020, **862**, 114000.

56 H. Zhang, Y. Guo, Z. Wu, Y. Wang, Y. Sun, X. Feng, H. Wang and G. Zhao, *J. Lumin.*, 2020, 117864.

57 A. J. Kronemeijer, E. Gili, M. Shahid, J. Rivnay, A. Salleo, M. Heeney and H. Sirringhaus, *Adv. Mater.*, 2012, **24**, 1558–1565.

58 Z. Chen, W. Li, M. A. Sabuj, Y. Li, W. Zhu, M. Zeng, C. S. Sarap, M. M. Huda, X. Qiao, X. Peng *et al.*, *Nature Communications*, 2021, **12**, 1–10.

59 M. J. Frisch, G. W. Trucks, H. B. Schlegel, G. E. Scuseria, M. A. Robb, J. R. Cheeseman, G. Scalmani, V. Barone, G. A. Petersson, H. Nakatsuji, X. Li, M. Caricato, A. V. Marenich, J. Bloino, B. G. Janesko, R. Gomperts, B. Mennucci, H. P. Hratchian, J. V. Ortiz, A. F. Izmaylov, J. L. Sonnenberg, D. Williams-Young, F. Ding, F. Lipparini, F. Egidi, J. Goings, B. Peng, A. Petrone, T. Henderson, D. Ranasinghe, V. G. Zakrzewski, J. Gao, N. Rega, G. Zheng, W. Liang, M. Hada, M. Ehara, K. Toyota, R. Fukuda, J. Hasegawa, M. Ishida, T. Nakajima, Y. Honda, O. Kitao, H. Nakai, T. Vreven, K. Throssell, J. A. Montgomery, Jr., J. E. Peralta, F. Ogliaro, M. J. Bearpark, J. J. Heyd, E. N. Brothers, K. N. Kudin, V. N. Staroverov, T. A. Keith, R. Kobayashi, J. Normand, K. Raghavachari, A. P. Rendell, J. C. Burant, S. S. Iyengar, J. Tomasi, M. Cossi, J. M. Millam, M. Klene, C. Adamo, R. Cammi, J. W. Ochterski, R. L. Martin, K. Morokuma, O. Farkas, J. B. Foresman and D. J. Fox, *Gaussian 16 Revision B.01*, 2016, Gaussian Inc. Wallingford CT.

60 A. D. Becke, *J. Chem. Phys.*, 1993, **98**, 1372–1377.

61 P. Stephens, F. Devlin, C. Chabalowski and M. J. Frisch, *J. Phys. Chem.*, 1994, **98**, 11623–11627.

62 D. Feller, *J. Comput. Chem.*, 1996, **17**, 1571–1586.

63 K. L. Schuchardt, B. T. Didier, T. Elsethagen, L. Sun, V. Gurumoorthi, J. Chase, J. Li and T. L. Windus, *J. Chem. Inf. Model.*, 2007, **47**, 1045–1052.

64 M. M. Francl, W. J. Pietro, W. J. Hehre, J. S. Binkley, M. S. Gordon, D. J. DeFrees and J. A. Pople, *J. Chem. Phys.*, 1982, **77**, 3654–3665.

65 J. B. Foresman and Æ. Frisch, *Exploring Chemistry with Electronic Structure Methods*, Gaussian, Gaussian Inc. Wallingford CT, 3rd edn, 2015.

66 L. Noodleman, *J. Chem. Phys.*, 1981, **74**, 5737–5743.

67 E. D. Glendening, C. R. Landis and F. Weinhold, *J. Comput. Chem.*, 2013, **34**, 1429–1437.

68 P. v. R. Schleyer, M. Manoharan, Z.-X. Wang, B. Kiran, H. Jiao, R. Puchta and N. J. van Eikema Hommes, *Org. Lett.*, 2001, **3**, 2465–2468.

69 R. Ditchfield, *Mol. Phys.*, 1974, **27**, 789–807.

70 R. Herges and D. Geuenich, *J. Phys. Chem. A*, 2001, **105**, 3214–3220.

71 T. A. Keith and R. F. Bader, *Chem. Phys. Lett.*, 1993, **210**, 223–231.

72 S. Klod and E. Kleinpeter, *J. Chem. Soc., Perkin. Trans. 2*, 2001, 1893–1898.

73 J. Kruszewski and T. Krygowski, *Tetrahedron Lett.*, 1972, **13**, 3839–3842.

74 T. M. Krygowski and M. K. Cyrański, *Chem. Rev.*, 2001, **101**, 1385–1420.

75 T. M. Henderson, A. F. Izmaylov, G. Scalmani and G. E. Scuseria, *J. Chem. Phys.*, 2009, **131**, 044108.

76 T. Stein, H. Eisenberg, L. Kronik and R. Baer, *Phys. Rev. Lett.*, 2010, **105**, 266802.

77 W. Humphrey, A. Dalke and K. Schulten, *J. Molec. Graphics*, 1996, **14**, 33–38.

78 Y. Liu, H. Phan, T. S. Herng, T. Y. Gopalakrishna, J. Ding and J. Wu, *Chem. Asian J.*, 2017, **12**, 2177–2182.

79 A. Thomas, K. Bhanuprakash and K. K. Prasad, *J. Phys. Org. Chem.*, 2011, **24**, 821–832.

80 J. D. Yuen, M. Wang, J. Fan, D. Sheberla, M. Kemei, N. Banerji, M. Scarongella, S. Valouch, T. Pho and R. Kumar, *J. Polym. Sci. A Pol. Chem.*, 2015, **53**, 287–293.

81 W. Wang, L. Ge, G. Xue, F. Miao, P. Chen, H. Chen, Y. Lin, Y. Ni, J. Xiong and Y. Hu, *Chem. Commun.*, 2020, **56**, 1405–1408.

82 T. Yanai, D. P. Tew and N. C. Handy, *Chem. Phys. Lett.*, 2004, **393**, 51–57.

83 J.-D. Chai and M. Head-Gordon, *Phys. Chem. Chem. Phys.*, 2008, **10**, 6615–6620.

84 J. J. Dressler, M. Teraoka, G. L. Espejo, R. Kishi, S. Takamuku, C. J. Gómez-García, L. N. Zakharov, M. Nakano, J. Casado and M. M. Haley, *Nat. Chem.*, 2018, **10**, 1134–1140.

85 G. E. Rudebusch, J. L. Zafra, K. Jorner, K. Fukuda, J. L. Marshall, I. Arrechea-Marcos, G. L. Espejo, R. P. Ortiz, C. J. Gómez-García and L. N. Zakharov, *Nat. Chem.*, 2016, **8**, 753–759.

86 M. Nakano, *Excitation energies and properties of open-shell singlet molecules: applications to a new class of molecules for nonlinear optics and singlet fission*, Springer, 2014.

87 J. Towns, T. Cockerill, M. Dahan, I. Foster, K. Gaither, A. Grimshaw, V. Hazlewood, S. Lathrop, D. Lifka, G. D. Peterson *et al.*, *Comput Sci. Eng.*, 2014, **16**, 62–74.